Available online at www.sciencedirect.com
SCIENCE DIRECT®
PERGAMON
International Journal of Multiphase Flow 29 (2003) 461–474
International Journal of Multiphase Flow
www.elsevier.com/locate/ijmulflow

Numerical simulation of a particle-laden plasma flow in a complex configuration under an electromagnetic field ☆

Takehiko Sato [a,*], Oleg P. Solonenko [b], Hideya Nishiyama [a]

[a] *Institute of Fluid Science, Tohoku University, 2-1-1 Katahira, Aoba-ku, Sendai 980-8577, Japan*
[b] *Institute of Theoretical and Applied Mechanics, Siberian Branch of the Russian Academy of Sciences, 4/1, Institutskaya av., Novosibirsk 630090, Russia*

Received 1 June 2001; received in revised form 5 November 2002

Abstract

Numerical simulation was conducted to clarify the electromagnetic thermofluid fields of a particle-laden compressible plasma flow in a complex configuration, as well as the characteristics of the injected fine particles in the plasma flow. The effects of an applied radio-frequency (RF) electromagnetic field, particle size and particle material on in-flight particle characteristics were clarified by use of a numerical model which took plasma compressibility and variable transport properties into consideration. Particle velocity was found to be strongly influenced by particle diameter. The heating rate of the Ni particle was the highest due to its lowest latent heat of melting. It was possible to efficiently control particle temperature by heating of the plasma flow with an RF electromagnetic field applied to the nozzle. Finally, particle phase condition was drawn in terms of the injection velocity and particle diameter for optimization of particle properties.
© 2003 Elsevier Science Ltd. All rights reserved.

Keywords: Plasma flow; Particulate flow; Electromagnetic field; Numerical simulation; Complex configuration; Phase change

1. Introduction

Plasma is regarded as a multifunctional fluid, because it is characterized by high energy density, chemical reactivity and variable transport properties. Therefore, plasma has been utilized for

☆ This paper was presented in the 4th International Conference on Multiphase Flow (ICMF-2001). The ICMF-2001 took place in New Orleans, USA during the week of May 27 to June 1, 2001 and was attended by 630 delegates representing 46 countries. Professor E.E. Michaelides was the chair of the conference.

* Corresponding author. Tel./fax: +81-22-217-5320.
E-mail address: sato@ifs.tohoku.ac.jp (T. Sato).

0301-9322/03/$ - see front matter © 2003 Elsevier Science Ltd. All rights reserved.
doi:10.1016/S0301-9322(02)00153-2

material processing, such as cutting, welding and spraying, and environmental treatments, such as decomposition of dioxin, freon and melting incombustible waste to reduce its volume. For example, Yamamoto and Jang (1999) reported the reduction of NO_x using corona discharge plasma. Sakano et al. (1999) and Ramachandran and Kikukawa (2000) investigated the recovery of heavy metals from flying ash and electroplating sludge, respectively, using thermal plasma.

McKelliget et al. (1982) investigated a steady turbulent plasma flow by numerical simulation. Chen and Pfender (1982) theoretically analyzed the unsteady thermal characteristics of particles in a plasma flow. Pfender (1989) investigated characteristics of in-flight particles in plasma spraying. Wei et al. (1987) numerically analyzed the characteristics of melting particles in a low pressure supersonic plasma flow. Heimann (1996) and Solonenko (1995) analyzed plasma spraying both experimentally and theoretically. Vardelle et al. (1982) reported experimental data on particle velocity and temperature in a plasma flow. Two-dimensional analysis of an radio-frequency (RF) inductive electromagnetic field was reported by Mostaghimi and Bolous (1989). Although Nam et al. (1996) and Nishiyama et al. (1999) presented models and simulations of particle-laden plasma in an electromagnetic field, a particle-laden plasma flow in a complex configuration and such a flow in an applied RF inductive electromagnetic field have not yet been investigated completely. Especially, the optimum particle injection conditions for purification of incineration ashes and plasma spraying have not yet been clarified in detail. Since plasma is an electrically conductive fluid, which is considered to be a functional fluid for control of the electromagnetic process, it is very important to clarify in detail the characteristics of particle-laden plasma flow in an electromagnetic field. The main objective of the present paper is to clarify compressible thermal plasma flow in a complex configuration under conditions of an RF induction electromagnetic field and the characteristics of fine particles injected into a plasma flow using a numerical model which takes compressibility and variable transport properties into consideration.

2. Numerical model

2.1. Assumptions

The numerical model is based on the following assumptions. (1) The DC plasma flow is treated only downstream of the arc region. (2) The plasma is a continuous, ideal gas in local thermodynamic equilibrium (LTE), which is optically thin and has variable thermodynamic and transport properties. (3) The flow, temperature and electromagnetic fields are two-dimensionally axisymmetric. (4) The magnetic Reynolds number is small. (5) All injected particles are spheres with the same diameter, and the internal temperature is uniform because the ratio between convection heat resistance and internal heat resistance, namely, the Bi number is low. (6) Only drag force acts on the particles. (7) The thermodynamic and transport properties of the particles in both the solid and liquid phases are functions of particle temperature. (8) Collisions between particles are neglected due to the dilute particle-loading condition. (9) There is one-way coupling between the dispersed phase and the carrier phase. (10) The nozzle and the chamber are electrically insulated. (11) The vector potential and the induction electric field have only azimuthal component.

2.2. Governing equations

Under the above-mentioned assumptions, the governing equations for plasma flow, particle and induction electromagnetic field are presented as follows:

2.2.1. Plasma flow

Continuity equation:

$$\frac{\partial \rho}{\partial t} + \operatorname{div}(\rho \boldsymbol{u}) = 0. \tag{1}$$

Momentum equations:

$$\frac{\partial(\rho \boldsymbol{u})}{\partial t} + \nabla \cdot (\rho \boldsymbol{u}\boldsymbol{u}) = -\nabla p + \nabla \cdot \bar{\bar{\tau}} + \boldsymbol{F}, \tag{2}$$

where the axial and radial Lorentz forces F_z and F_r and the viscous stress $\bar{\bar{\tau}}$ are given by

$$F_r = \frac{1}{2}\sigma \operatorname{Real}(E_\theta \overline{B}_z), \quad F_z = -\frac{1}{2}\sigma \operatorname{Real}\left(E_\theta \overline{B}_r\right) \tag{3}$$

and

$$\bar{\bar{\tau}} = \tau_{ij} = 2\mu\left(e_{ij} - \frac{1}{3}\delta_{ij}(\nabla \cdot \boldsymbol{u})\right). \tag{4}$$

Here, e_{ij} and δ_{ij} are the strain rate tensor and the Kronecker delta, respectively.

Energy equation:

$$\frac{\partial}{\partial t} e + \nabla \cdot [(e + p)\boldsymbol{u}] = \nabla \cdot (\lambda \nabla T) + \Phi_{\mathrm{D}} + Q_{\mathrm{j}} - Q_r, \tag{5}$$

$$e = \rho\left(C_v T + \frac{\boldsymbol{u} \cdot \boldsymbol{u}}{2}\right), \quad Q_{\mathrm{j}} = \boldsymbol{j} \cdot \boldsymbol{E} = \frac{\sigma}{2}\left[E_\theta \overline{E}_\theta\right] \tag{6}$$

and

$$\Phi_{\mathrm{D}} = 2\mu\left(e_{ij} - \frac{1}{3}\delta_{ij}(\nabla \cdot \boldsymbol{u})\right)^2, \tag{7}$$

where e, Q_{j} and Φ_{D} are stagnant internal energy per unit volume, Joule heating and dissipation loss, respectively, as shown in Eqs. (6) and (7). Q_r is radiation loss given by approximation curve fittings from the experimental radiation data reported by Evans and Tankin (1967).

Equation of state:

$$p = \rho R T. \tag{8}$$

In the equations for plasma flow, $\boldsymbol{u}$, p, $\boldsymbol{E}$, $\boldsymbol{B}$, T and C_v represent plasma velocity, pressure, electric field intensity, magnetic flux density, plasma temperature and specific heat at constant volume, respectively. ρ, σ, μ and λ represent density, electrical conductivity, viscosity and thermal conductivity, respectively.

2.2.2. Particle

Equation of motion:

$$m_{\mathrm{p}}\frac{\mathrm{d}\boldsymbol{u}_{\mathrm{p}}}{\mathrm{d}t}=\frac{\pi}{8}d_{\mathrm{p}}^{2}\rho C_{\mathrm{Df}}\left(\boldsymbol{u}-\boldsymbol{u}_{\mathrm{p}}\right)\left|\boldsymbol{u}-\boldsymbol{u}_{\mathrm{p}}\right|. \tag{9}$$

The drag coefficient is reported by Crowe et al. (1977). Accounted for are variable transport properties in the particle boundary layer, as shown by Pfender and Lee (1985):

$$C_{\mathrm{Df}}=\frac{24}{Re_{\mathrm{p}}}\left(1+0.15Re_{\mathrm{p}}^{0.687}\right)\left(\frac{\rho_{\infty}\mu_{\infty}}{\rho_{\mathrm{s}}\mu_{\mathrm{s}}}\right)^{-0.45}, \tag{10}$$

where the particle Reynolds number Re_{p} and the film temperature T_{f} are respectively defined as

$$Re_{\mathrm{p}}=\frac{\rho_{\mathrm{f}}d_{\mathrm{p}}\left|\boldsymbol{u}-\boldsymbol{u}_{\mathrm{p}}\right|}{\mu_{\mathrm{f}}}\quad\text{and}\quad T_{\mathrm{f}}=\frac{T_{\infty}+T_{\mathrm{p}}}{2}. \tag{11}$$

Heat balance equation:

$$m_{\mathrm{p}}c_{\mathrm{p}}\frac{\mathrm{d}T_{\mathrm{p}}}{\mathrm{d}t}=\pi d_{\mathrm{p}}^{2}\left[h_{\mathrm{f}}(T_{\infty}-T_{\mathrm{p}})-\varepsilon_{\mathrm{p}}\sigma_{\mathrm{SB}}(T_{\mathrm{p}}^{4}-T_{\mathrm{a}}^{4})\right]\quad(T_{\mathrm{p}}<T_{m}\text{ and }T_{m}<T_{\mathrm{p}}<T_{b}). \tag{12}$$

The heat transfer coefficient presented by Lee et al. (1985) incorporates the variable transport properties in the particle boundary layer.

$$h_{\mathrm{f}}=\frac{\lambda_{\mathrm{f}}}{d_{\mathrm{p}}}(2+0.6Re_{\mathrm{p}}^{1/2}Pr^{1/3})\left(\frac{\rho_{\infty}\mu_{\infty}}{\rho_{\mathrm{s}}\mu_{\mathrm{s}}}\right)^{0.6}\left(\frac{C_{\mathrm{p}\infty}}{C_{\mathrm{ps}}}\right)^{0.38}, \tag{13}$$

where Prandtl number Rr is defined using film temperature.

$$Pr=\frac{C_{\mathrm{pf}}\mu_{\mathrm{f}}}{\lambda_{\mathrm{f}}},\quad T_{\mathrm{f}}=\frac{T_{\infty}+T_{\mathrm{p}}}{2}. \tag{14}$$

The phase change of a particle is evaluated from the following criteria.

The particle is fully melted when

$$\int_{0}^{t}Q_{n}\,\mathrm{d}t\geqslant m_{\mathrm{p}}\int_{T_{0}}^{T_{\mathrm{pm}}}c_{\mathrm{p}}\,\mathrm{d}T+m_{\mathrm{p}}L_{\mathrm{pm}}\equiv Q_{\mathrm{pm}}\quad(T_{\mathrm{p}}\geqslant T_{\mathrm{pm}}). \tag{15}$$

The particle is fully evaporated when

$$\int_{0}^{t}Q_{n}\,\mathrm{d}t\geqslant Q_{\mathrm{pm}}+m_{\mathrm{p}}\int_{T_{\mathrm{pm}}}^{T_{\mathrm{bm}}}c_{\mathrm{p}}\,\mathrm{d}T+m_{\mathrm{p}}L_{\mathrm{pb}}. \tag{16}$$

In the equations for particle motion and heat transfer, m_{p}, $\boldsymbol{u}_{\mathrm{p}}$, d_{p}, Re_{p}, c_{p}, T_{p}, T_{pm}, L_{pm} and L_{pb} respectively represent the mass, velocity, diameter, Reynolds number, specific heat, temperature, melting point, latent heat of melting and latent heat of boiling of the particle, and T_{a} represents ambient temperature. The ambient temperature is the room temperature. μ, ε_{p} and σ_{SB} represent viscosity, particle emissivity and Stefan–Boltzmann's constant, respectively. Subscripts s, ∞ and f correspond to particle surface, bulk and film, respectively. For example, parameters μ_{s} and μ_{∞} represent the viscosities of the plasma flow at the particle surface temperature and at the plasma temperature, respectively, the latter being unaffected by the boundary layer, around the particle.

Parameters ρ, T and C_p are defined by the same method as employed for μ_s and μ_∞. The transport properties are given by approximation of multiterms as a function of temperature as presented by Bilodeau and Gleizes (1997).

2.2.3. Induction electromagnetic field

The vector potential equation as presented by Mostaghimi and Bolous (1989),

$$\nabla^2 \boldsymbol{A}_c - i\mu_0 \sigma \omega \boldsymbol{A}_c = 0, \tag{17}$$

is derived from Maxwell's equations.

Electric field:

$$\boldsymbol{E}_c = -i\omega \boldsymbol{A}_c. \tag{18}$$

Magnetic field:

$$\boldsymbol{B}_c = \nabla \times \boldsymbol{A}_c, \tag{19}$$

where

$$\omega = 2\pi f_{RF}, \quad \boldsymbol{A}(\boldsymbol{r},t) = \boldsymbol{A}_c(\boldsymbol{r})e^{i\omega t}, \quad \boldsymbol{B}(\boldsymbol{r},t) = \boldsymbol{B}_c(\boldsymbol{r})e^{i\omega t}, \quad \boldsymbol{E}(\boldsymbol{r},t) = \boldsymbol{E}_c(\boldsymbol{r})e^{i\omega t}. \tag{20}$$

In the equations for the electromagnetic field, $\boldsymbol{A}$, $\boldsymbol{E}$, $\boldsymbol{B}$, f_{RF}, ω, μ_0 and i represent vector potential, electric field intensity, magnetic flux density, frequency of RF coil current, angular frequency, permeability of vacuum and imaginary unit, respectively.

2.3. Boundary conditions

The boundary conditions for the plasma jet and the induction electromagnetic field are given in terms of independent variables such as density, velocity and vector potential.

Nozzle inlet:

$$\rho = \rho_{in}, \quad u = u_{in}, \quad v = 0, \quad \frac{\partial \boldsymbol{A}_R}{\partial z} = \frac{\partial \boldsymbol{A}_I}{\partial z} = 0. \tag{21}$$

Axis:

$$\frac{\partial \rho}{\partial r} = 0, \quad \frac{\partial u}{\partial r} = 0, \quad v = 0, \quad \boldsymbol{A}_R = \boldsymbol{A}_I = 0. \tag{22}$$

Nozzle wall and outer wall:

$$\frac{\partial \rho}{\partial r} = 0 \text{ (horizontal wall)}, \quad \frac{\partial \rho}{\partial z} = 0 \text{ (vertical wall)}, \quad u = v = 0, \tag{23}$$

$$\boldsymbol{A}_R = \frac{\mu_o I}{2\pi}\sqrt{\frac{r_c}{r_w}}\sum_{i=1}^{\text{coil}} G(l_i) + \frac{\mu_o \omega}{2\pi}\sum_{j=1}^{\text{c.v.}}\sqrt{\frac{r_j}{r_w}}\sigma_j \boldsymbol{A}_{Ij} S_j G(l_j), \tag{24}$$

$$\boldsymbol{A}_I = -\frac{\mu_o \omega}{2\pi}\sum_{j=1}^{\text{c.v.}}\sqrt{\frac{r_j}{r_w}}\sigma_j \boldsymbol{A}_{Rj} S_j G(l_j).$$

Inner wall:

$$\frac{\partial \rho}{\partial r} = 0 \text{ (horizontal wall)}, \quad \frac{\partial \rho}{\partial z} = 0 \text{ (vertical wall)}, \quad u = v = 0, \quad A_R = A_I = 0. \tag{25}$$

Reactor exit:

$$\frac{\partial \rho}{\partial z} = 0, \quad \frac{\partial u}{\partial z} = \frac{\partial v}{\partial z} = 0, \quad p = p_{\text{operating}}, \quad \frac{\partial \boldsymbol{A}_R}{\partial z} = \frac{\partial \boldsymbol{A}_I}{\partial z} = 0. \tag{26}$$

When the flow is supersonic at the reactor exit, the pressure condition in Eq. (26) is neglected. Here, $\boldsymbol{A}_R$ and $\boldsymbol{A}_I$ represent the real part and the imaginary part of vector potential $\boldsymbol{A}$, respectively. r_c, r_w, S_j and $G(l_j)$ are coil radius, nozzle and chamber radius, cross section of the j_{th} control volume and function of complete elliptical integrals, respectively.

2.4. Numerical procedure

Fig. 1 shows a schematic of the complex computational domain. The configuration represents plasma spraying and the computational conditions are given in Table 1.

The governing equations for plasma flow are solved using the 3rd-order MUSCL type TVD method for the convective term as reported by Anderson et al. (1986) and the LU-SGS method for time integration as proposed by Yoon and Jameson (1988) to take the variation of plasma density into account, these methods being suitable for unsteady transonic or supersonic flows. Nishiyama et al. (1999) also showed that these methods are very suitable for a supersonic plasma flow near a

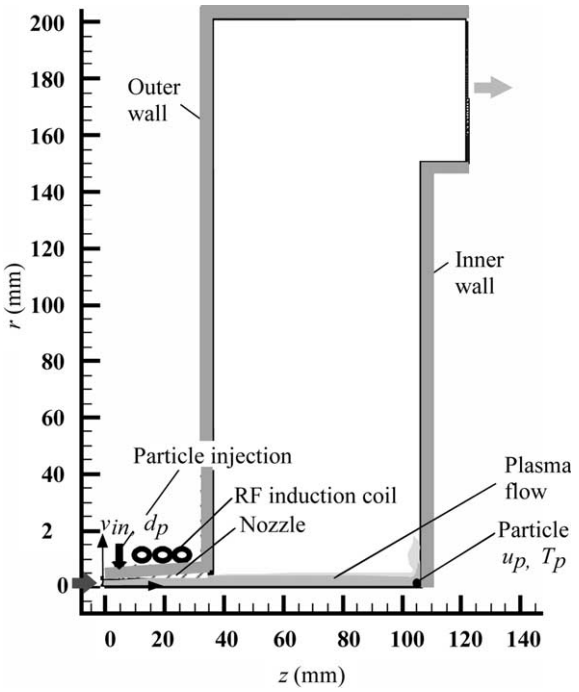

Fig. 1. Schematic of computational domain.

Table 1
Computational conditions

Working gas	Ar
Gas flow rate	0.1 g/s
DC torch input power	10 kW
RF power	6 kW
Frequency	13.56 MHz
Operating pressure	50 kPa
Nozzle angle	4.5°
Particle material	W, Ni, Al_2O_3
Particle diameter	10–100 μm
Particle injection velocity	0.0–8.0 m/s
RF induction coil	with/without

flat plate. The governing equations for the particle method are discretized by regarding them as the 1st-order differential equations. The plasma parameters at the particle position correspond to the value of the upper and center side node in the cell where the particle is located. The equations for the electromagnetic field are solved using the Pointing Jacobi method. The calculation domain includes a particle injection nozzle and a reactor having a 298×131 grid, but does not include a DC torch. Turbulent eddies larger than the cell size can be evaluated without introducing the turbulence model in this direct simulation.

3. Numerical results and discussion

3.1. Plasma characteristics

Fig. 2 shows the plasma axial velocity field (a) without and (b) with an RF electromagnetic field under the conditions of a discharge power of 10 kW and an operating pressure of 50 kPa. The plasma flow is accelerated in the nozzle due to the expansion effect. The flow impinges on the inner wall with some entrainment. The high velocity region is expanded from the nozzle exit under an applied RF electromagnetic field. However, the effect of an applied RF electromagnetic field on the plasma velocity is slight because the driving force accelerating the plasma flow depends on the pressure difference between the nozzle inlet and exit.

Fig. 3 shows the plasma temperature field (a) without RF and (b) with RF under the same operating conditions as mentioned above. Although the plasma velocity is high, the temperature is increased effectively in the downstream region by applying the RF electromagnetic field due to the active production of Joule heating. Although the inlet plasma temperature is high, it decreases with the increase in the plasma velocity due to the conservation of the stagnant enthalpy as shown by Eq. (6).

3.2. Particle characteristics

Fig. 4 shows the instantaneous dispersion of particles for W, Ni and Al_2O_3 (a) without RF and (b) with RF under the same discharge power and the same operating pressure. Different dispersions

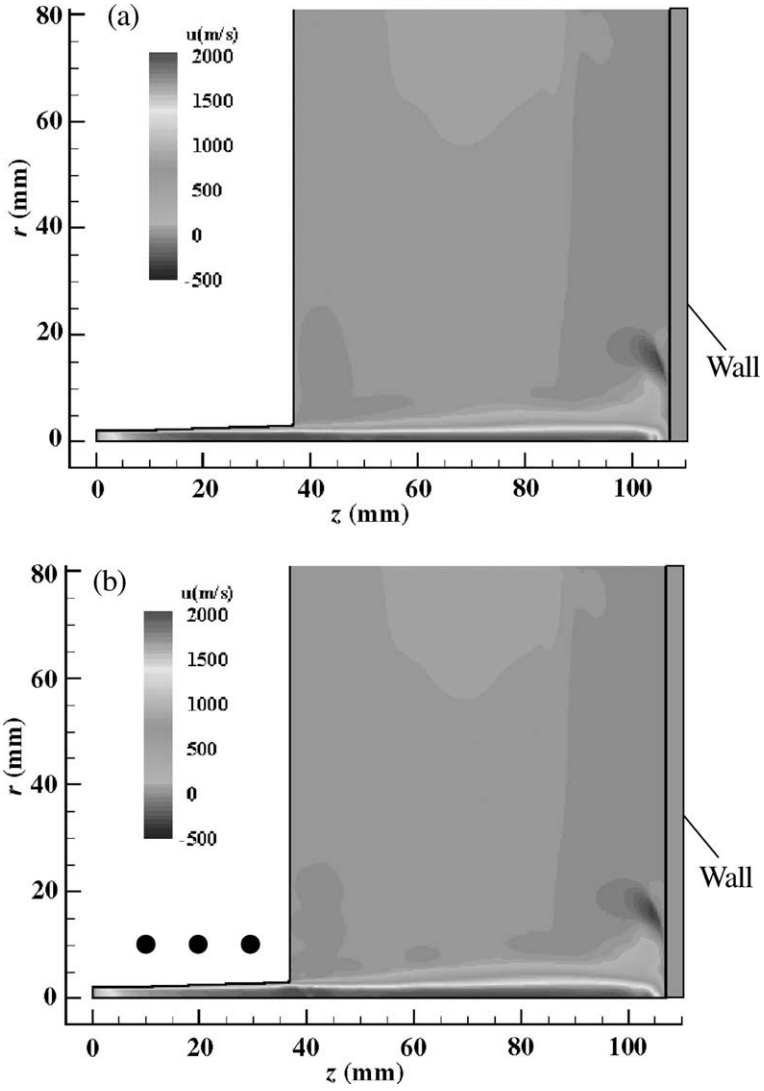

Fig. 2. Plasma axial velocity: (a) without RF, (b) with RF.

are observed among the particle materials because of the different densities. Dispersed fluctuations are caused by the unsteady effects of the plasma jet. Furthermore, larger fluctuation can be observed near the plasma jet fringe. Sato and Nishiyama (2000) also reported in detail that particle trajectories depend on the injection particle velocity, operating pressure, diffusive angle of the nozzle and particle diameter in a straight pipe. The optimum diffusive angle and operating pressure were clarified to obtain high impact particle velocity and temperature.

Fig. 5 shows the axial evolution of particle velocities of W for different diameters, namely, 20, 30 and 60 μm. The radial injection velocity of particles is 2.5 m/s at $z = 5$ mm. The particle velocity is greater for smaller particles due to their low inertia. The effect of application of an RF

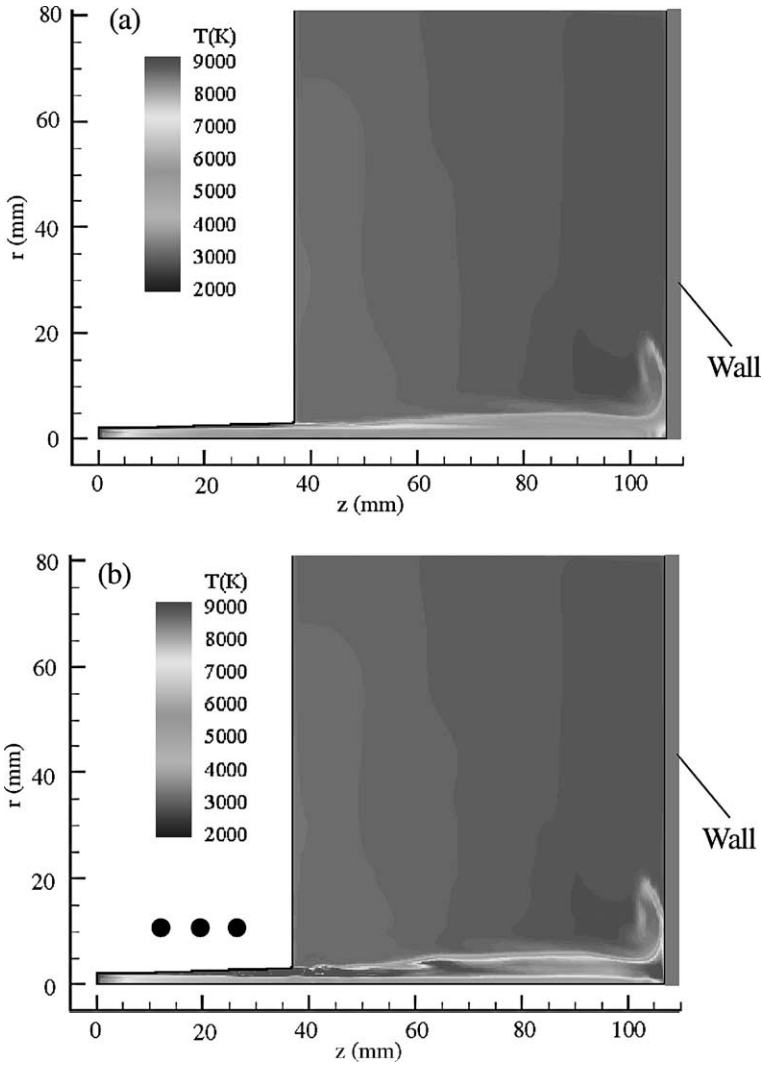

Fig. 3. Plasma temperature: (a) without RF, (b) with RF.

electromagnetic field on particle velocity is insignificant in this case which corresponds to the plasma velocity as shown in Fig. 2. The particle momentum is important in plasma spraying to increase the adhesion of coating on the substrate. Therefore, it is necessary to clarify the velocity of the particle prior to its impact on the inner wall.

Fig. 6 shows the correlation between the particle injection velocity and particle diameter for high and low particle impact velocities without RF. This means, for example, that an Al_2O_3 particle is accelerated up to more than 450 m/s prior to impact under conditions in the left-hand portion of the figure. The conditions for the right-hand portion of the figure show that the particle impact velocity is less than 250 m/s. The particle impact velocity strongly depends on both the particle diameter and the material density. Since the density of an Al_2O_3 particle is the smallest

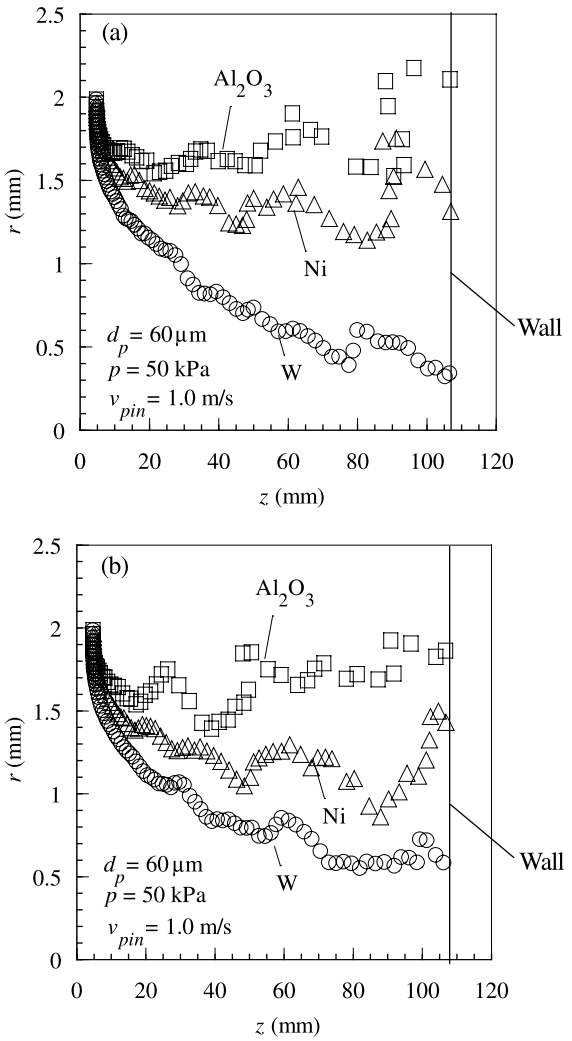

Fig. 4. Instantaneous dispersion of particles: (a) without RF, (b) with RF.

among the materials, the line showing 450 m/s is located at larger particle diameters. When the particle injection velocity is very low, the particle impact velocity becomes lower for smaller particles, because they cannot reach the high velocity region near the center axis of the plasma.

Fig. 7 shows the axial evolution of particle temperatures for W, Ni and Al_2O_3. The particle temperature increases rapidly up to the melting temperature. The heating rate of the Ni particle is greater than those of the W and Al_2O_3 particles. It is shown that the heating rate of the particles increase effectively when an RF electromagnetic field is applied because of the greater heat exchange with the plasma jet heated by Joule heating. It is also important to clarify the liquid phase conditions of the impact particles, because their particle solidification is one of the key processes which determine the coating properties in plasma spraying.

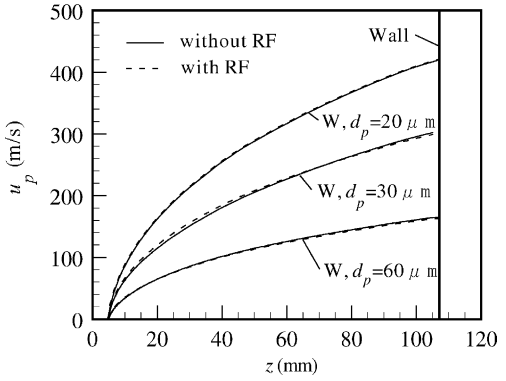

Fig. 5. Axial evolutions of W particle velocities with RF and without RF.

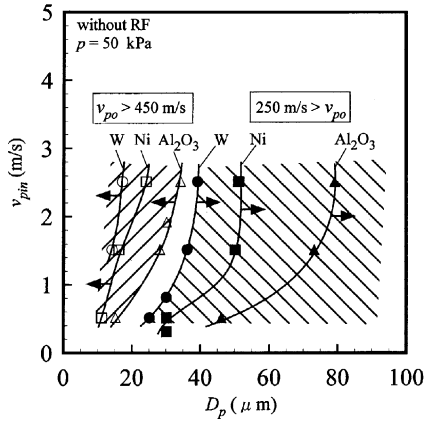

Fig. 6. Conditions of the particle injection velocity and particle diameter for high and low particle impact velocities without RF.

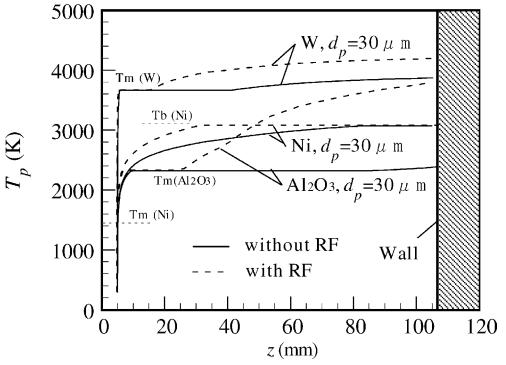

Fig. 7. Axial evolutions of particle temperatures with RF and without RF.

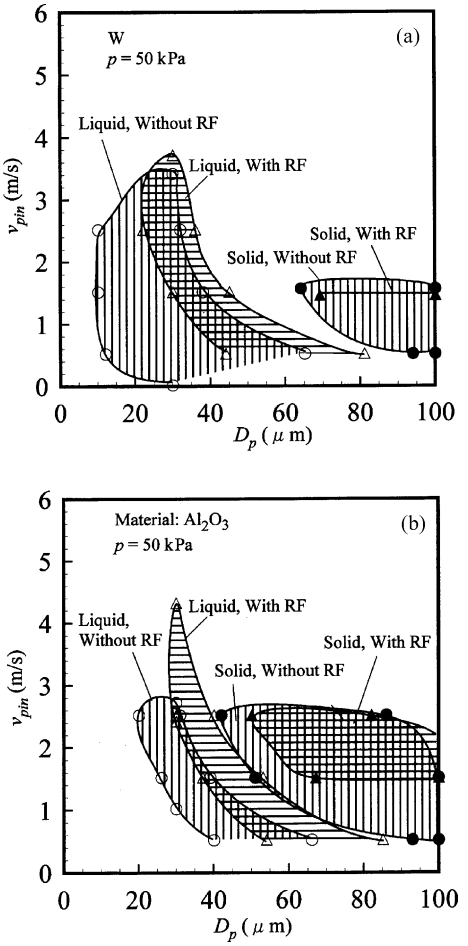

Fig. 8. Solid and liquid phase conditions of impact particles with and without RF: (a) W, (b) Al_2O_3.

Fig. 8 shows the solid and liquid phase conditions of the impact particles with and without RF, (a) W and (b) Al_2O_3, respectively. The liquid phase region with RF is shifted to the larger particle diameter region by the effect of RF electromagnetic heating. This implies that the applied RF electromagnetic field is an effective means of controlling the solid and liquid phases of the in-flight particles without changing the particle injection velocity and particle diameter. Compared with the solid region of W, that of Al_2O_3 is observed in a wide range of diameters and of injection velocities despite the smaller liquid phase region, because Al_2O_3 has larger specific heat and lower boiling points.

4. Conclusions

Important control parameters and optimum operating conditions for in-flight particles in a compressible plasma flow through a complex configuration under conditions of an electromag-

netic field were clarified by numerical simulation. The main results obtained can be summarized as follows:

(1) Particle temperature is strongly affected by the plasma temperature. The latter can be increased effectively by applying an RF electromagnetic field to the nozzle due to active Joule heating.
(2) Particle dispersion depends on the material density.
(3) Particle impact velocity is influenced by its diameter and the material density via particle mass.
(4) The heating rate of the Ni particle is the highest due to its lowest latent heat of melting.
(5) Particle phase change is effectively controlled by its diameter, injection velocity and the applied RF electromagnetic field. Especially, the optimum conditions to change to the liquid phase depend on the kind of material.

Acknowledgements

The present study was partially supported by the Japan Society for Promotion of Science. The numerical simulation was conducted using the supercomputer Origin2000 at the Institute of Fluid Science, Tohoku University.

References

Anderson, W.K., Thomas, J.L., Leer, B.V., 1986. Comparison of finite volume flux vector splittings for the Euler equations. AIAA J. 24, 1452–1460.

Bilodeau, J.F., Gleizes, A., 1997. Plasma Chem. Plasma Process. 16, 605–634.

Chen, X., Pfender, E., 1982. Unsteady heating and radiation effects of small particles in a thermal plasma. Plasma Chem. Plasma Process. 2, 293–316.

Crowe, C.T., Sharma, M.P., Stock, D.E., 1977. The particle source-in cell (PSI-CELL) model for gas-droplet flows. J. Fluids Eng. 99, 325–332.

Evans, D.L., Tankin, R.S., 1967. Measurement of emission and absorption of radiation by an argon plasma. Phys. Fluids 10, 1137–1144.

Heimann, R.B., 1996. Plasma-Spray Coating. VCH Publishers, pp. 1–15.

Lee, Y.C., Chyou, Y.P., Pfender, E., 1985. Particle dynamics and particle heat and mass transfer in thermal plasmas, Part II. Particle heat and mass transfer in thermal plasmas. Plasma Chem. Plasma Process. 5, 391–414.

McKelliget, J., Szekely, J., Vardelle, M., Fauchais, P., 1982. Temperature and velocity fields in a gas stream exiting a plasma torch. A mathematical model and its experimental verification. Plasma Chem. Plasma Process. 2, 317–332.

Mostaghimi, J., Bolous, M.I., 1989. Two-dimensional electromagnetic field effects in induction plasma modelling. Plasma Chem. Plasma Process. 9, 25–44.

Nam, S.W., Nishiyama, H., Kamiyama, S., 1996. Numerical analysis on plasma spraying in a DC-RF hybrid plasma reactor. JSME Int. J., Ser. B 39, 134–140.

Nishiyama, H., Kuzuhara, M., Solonenko, O.P., Kamiyama, S., 1999. Numerical modeling of an impinging and compressible dusted plasma jet controlled by a magnetic field. Plasma Chem. Plasma Process. 19, 363–381.

Pfender, E., 1989. Particle behavior in thermal plasmas. Plasma Chem. Plasma Process. 9, 167S–194S.

Pfender, E., Lee, Y.C., 1985. Particle dynamics and particle heat and mass transfer in thermal plasmas. Part I. The motion of a single particle without thermal effects. Plasma Chem. Plasma Process. 5, 211–237.

Ramachandran, K., Kikukawa, N., 2000. Plasma in-flight treatment of electroplating sludge. Vacuum 59, 244–251.

Sato, T., Nishiyama, H., 2000. Numerical simulation of particle-laden plasma flow in a pipe under an RF electromagnetic field. Trans. JSME, Ser. B 66, 1295–1302, in Japanese.

Sakano, M., Watanabe, T., Tanaka, M., 1999. Application of radio-frequency thermal plasmas to treatment of fly ash. In: Proc. 14th Int. Symp. Plasma Chem., V, pp. 2495–2500.

Solonenko, O.P., 1995. State-of-the art of thermophysical fundamentals of plasma spraying. In: Thermal Plasma and New Materials Technology, vol. 2. Cambridge Interscience Press, pp. 7–96.

Vardelle, A., Vardelle, M., Fauchais, P., 1982. Influence of velocity and surface temperature of alumina particles on the properties of plasma sprayed coatings. Plasma Chem. Plasma Process. 2, 255–291.

Wei, D.Y.C., Farouk, B., Apelian, D., 1987. Melting powder particles in a low-pressure plasma jet. J. Heat Transf. 109, 971–976.

Yamamoto, T., Jang, B.W.-L., 1999. Aerosol generation and decomposition of CFC-113 by the ferroelectric plasma reactor. IEEE Trans. Ind. Appl. 35, 736–742.

Yoon, S., Jameson, A., 1988. Lower–upper symmetric-Gauss–Seidel method for the Euler and Navier–Stokes equations. AIAA J. 26, 1025–1026.